

# Rashba Effect and Raman Spectra of $\text{Ti}_2\text{O}/\text{PtS}_2$ Heterostructure

Shahid Sattar\* and J. Andreas Larsson\*

*Applied Physics, Division of Materials Science, Department of Engineering Sciences and  
Mathematics, Luleå University of Technology, Luleå SE-97187, Sweden*

E-mail: shahid.sattar@ltu.se; andreas.1.larsson@ltu.se

Phone: +46 (0)920 491930

## Abstract

The possibility to achieve charge-to-spin conversion via Rashba spin-orbit effects provide stimulating opportunities toward the development of nanoscale spintronics. Here we use first-principles calculations to study the electronic and spintronic properties of  $\text{Tl}_2\text{O}/\text{PtS}_2$  heterostructure, for which we have confirmed the dynamical stability by its positive phonon frequencies. An unexpectedly high binding energy of -0.38 eV per unit cell depicts strong interlayer interactions between  $\text{Tl}_2\text{O}$  and  $\text{PtS}_2$ . Interestingly, we discover Rashba spin-splitting's (with large  $\alpha_R$  value) in the valence band of  $\text{Tl}_2\text{O}$  stemming from interfacial spin-orbit effects caused by  $\text{PtS}_2$ . The role of van der Waals binding on the orbital rearrangements has been studied using electron localization function and atomic orbital projections, which explains in detail the electronic dispersion near the Fermi level. Moreover, we explain the distinct band structure alignment in momentum space but separation in real space of  $\text{Tl}_2\text{O}/\text{PtS}_2$  heterostructure. Since 2D  $\text{Tl}_2\text{O}$  still awaits experimental confirmation, we calculate, for the first time, the Raman spectra of pristine  $\text{Tl}_2\text{O}$  and the  $\text{Tl}_2\text{O}/\text{PtS}_2$  heterostructure and discuss peak positions corresponding to vibrational modes of the atoms. These findings offer a promising avenue to explore spin physics for potential spintronics applications via 2D heterostructures.

## Introduction

Spin-orbit effects in two-dimensional (2D) materials are of central importance for designing next-generation spintronic, valleytronic and spin-logic memory devices. Transition-metal dichalcogenides (TMDCs) such as  $\text{MoS}_2$ , in their pristine form and in proximity to other 2D materials, have been extensively utilized in such applications owing to their large spin-orbit strength and other promising features.<sup>1-4</sup> In this context, the Rashba spin-orbit effects (or simply Rashba effect) are of particular interest because it enables charge-to-spin conversion in a non-magnetic material by lifting spin-degeneracy along the momentum-axis without

the need of an external magnetic field.<sup>5,6</sup> The effect is observed experimentally in a variety of materials (e.g., in metal surfaces,<sup>7-14</sup> bulk materials,<sup>15-18</sup> perovskites,<sup>19-21</sup> topological insulators,<sup>22-24</sup> oxides<sup>25</sup> and 2D materials<sup>26,27</sup>) with a continued surge to achieve better control of the spin degree of freedom of electrons in new materials. Moreover, the possibility to build lateral and vertical 2D heterostructures without the constraints of lattice matching further broadens the scope of new discoveries and realization of novel phenomenon.

Monolayer  $\text{Tl}_2\text{O}$  is a recently proposed 2D metal-oxide semiconductor with cleavage energy comparable to well-known TMDCs.<sup>28</sup> Several theoretical studies highlighted its potential in catalysis,<sup>29</sup> valleytronics,<sup>30</sup> and especially in thermoelectrics<sup>31,32</sup> due to the ultralow lattice thermal conductivity.<sup>33</sup> Bulk  $\text{Tl}_2\text{O}$  crystallizes in the 1T-phase with its cousin polytype also existing in 2H-phase albeit higher in energy<sup>34</sup> thus favoring the synthesis of the former due to energetic reasons. While 2D  $\text{Tl}_2\text{O}$  still awaits experimental realization, a 2D thallene was recently fabricated on  $\text{NiSi}_2/\text{Si}(111)$  substrate experiencing a strong tensile strain due to the large lattice mismatch.<sup>35</sup> It is therefore extremely critical to select an appropriate material capable to host  $\text{Tl}_2\text{O}$  in its most stable form (without causing detrimental effects to its structure and properties) and permits usage in advanced applications.

In the present study, we use electronic structure theory calculations to demonstrate that 1T- $\text{Tl}_2\text{O}$  in heterostructure with the lattice-matched  $\text{PtS}_2$  has multiple advantages: 1) The heterostructure is dynamically stable as confirmed by the phonon band structure showing positive frequencies throughout the Brillouin zone. 2) An unusually high binding energy of -0.38 eV (per unit cell) depicts strong attachment between  $\text{Tl}_2\text{O}$  and  $\text{PtS}_2$  with structural features of both materials largely remain intact. 3) We observe giant Rashba spin-splittings with large Rashba ( $\alpha_R$ )-parameter in the  $\text{Tl}_2\text{O}/\text{PtS}_2$  heterostructure compared to previously studied heterostructures of 2D materials. These findings are further confirmed by spin-texture plots with detailed analysis of the electron localization function (ELF) and electronic density of states (DOS) in connection with the interfacial spin-orbit effects. We also note that for a small biaxial tensile strain, the characteristic Rashba splittings near the Fermi level is

maintained. Furthermore, to expedite a quick experimental confirmation of our work, we present for the first time the Raman spectra of pristine  $\text{Tl}_2\text{O}$  and the  $\text{Tl}_2\text{O}/\text{PtS}_2$  heterostructure. Owing to the importance of spin generation and charge-to-spin conversion, our results provide crucial insights into  $\text{Tl}_2\text{O}$  heterostructures that offers rich spin-valley physics and potential within spintronics applications.

## Computational method

First-principles calculations have been performed using density functional theory (DFT) with projector augmented waves<sup>36,37</sup> as implemented in the Vienna Ab-initio Simulation Package.<sup>38</sup> We used the generalized gradient approximation in the Perdew-Burke-Ernzerhof parametrization to describe the exchange-correlation effects, with a plane wave cutoff energy set to 450 eV. The van der Waals interactions have been taken into account using the DFT-D3 method.<sup>39</sup> A gamma-centered  $12 \times 12 \times 1$  k-mesh was employed for the structural relaxation and in the self-consistent calculations, Brillouin zone integration was performed using a dense  $20 \times 20 \times 1$  k-mesh. Due to the involvement of heavy elements, spin-orbit effects were included in the band structure and density-of-states (DOS) calculations. To calculate the phonon band structure, we used the Phonopy package<sup>40</sup> using a  $4 \times 4 \times 1$  supercell of  $\text{Tl}_2\text{O}/\text{PtS}_2$  heterostructure with a  $4 \times 4 \times 1$  k-mesh. Moreover, 2D spin-textures were computed by setting up a 2D k-mesh ( $k_x \times k_y : 30 \times 30$ ) centered at the gamma-point ( $k_z = 0$ ). For the iterative solution of the Kohn-Sham equations, we achieved an energy convergence of  $10^{-6}$  eV and a force convergence of  $10^{-3}$  eV/Å in our calculations. To avoid out-of-plane periodic image interactions, we have also used a 15 Å thick layer of vacuum. The Raman spectra of  $\text{Tl}_2\text{O}$  and the  $\text{Tl}_2\text{O}/\text{PtS}_2$  heterostructure were computed by calculating the derivative of the macroscopic dielectric tensor with respect to the mode coordinates using VASP and Phonopy<sup>40</sup> assisted *raman-sc* python package.<sup>41</sup> The results were plotted using the Pyprocar<sup>42</sup> and Matplotlib software packages.<sup>43</sup>

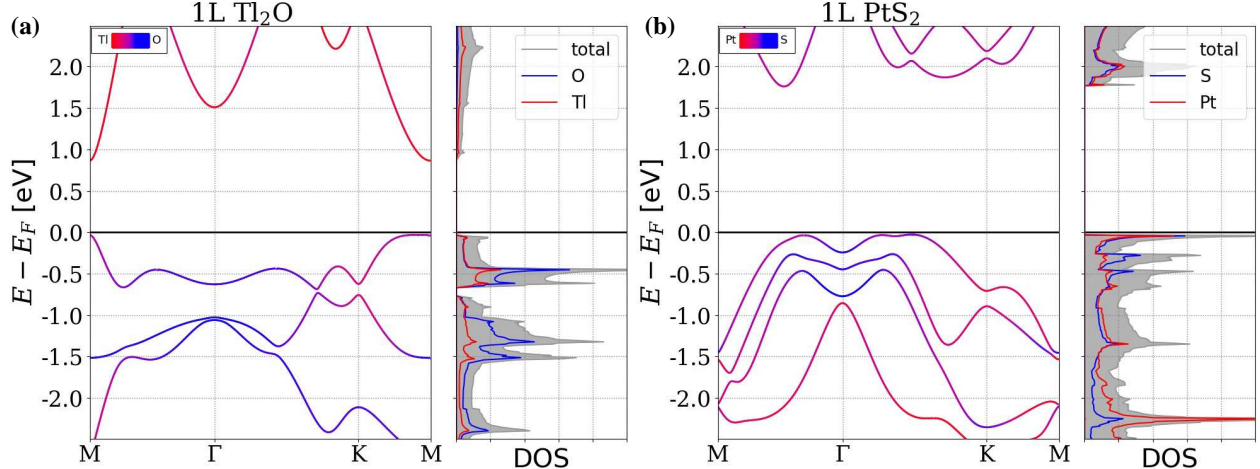


Figure 1: Atom-projected electronic band structure and density-of-states (DOS) of monolayer (1L) (a)  $\text{Tl}_2\text{O}$  and (b)  $\text{PtS}_2$ , respectively. Spin-orbit coupling is included in both cases.

## Results and Discussion

Monolayer  $\text{Tl}_2\text{O}$  and  $\text{PtS}_2$  both adopts 1T-phase trigonal prismatic geometry with an oxygen (O)(or platinum (Pt)) atom covalently bonded to two thallium (Tl) (or sulphur (S)) atoms, respectively. The optimized lattice parameter of  $3.56 \text{ \AA}$  ( $3.58 \text{ \AA}$ ) for  $\text{Tl}_2\text{O}$  ( $\text{PtS}_2$ ) and band gaps of  $0.90 \text{ eV}$  ( $1.80 \text{ eV}$ ), respectively, are in close agreement to the existing reports.<sup>33,44</sup> Because of the lattice matched crystal structures, the possibility of epitaxial growth of  $\text{Tl}_2\text{O}$  on  $\text{PtS}_2$  is anticipated. The atom-projected electronic band structure and density of states (DOS) for pristine monolayer  $\text{Tl}_2\text{O}$  and  $\text{PtS}_2$  are shown in Figure 1(a-b). Looking at the valence band of  $\text{Tl}_2\text{O}$ , it consists of mixed Tl and O atomic states whereas the conduction band mainly has Tl contributions, as depicted in the atom-projected DOS shown in Figure 1a. On the other hand,  $\text{PtS}_2$  show mixed contribution of Pt and S atomic states in both valence and conduction bands, as shown in Figure 1b.

In order to built  $\text{Tl}_2\text{O}/\text{PtS}_2$  heterostructures, we considered different lateral stackings by selecting multiple sites on  $\text{PtS}_2$ . Figure 2 shows top and side views of three such stacking configurations. In Figure 2a/d the Tl atom lie exactly on top of S atoms. To scan different possible stackings, we traversed along  $a$ - and  $b$ -axes, and also considered the inversion of  $\text{Tl}_2\text{O}$  as shown in Figure 2(b/e). The stacking where O atoms lie exactly on top of top S

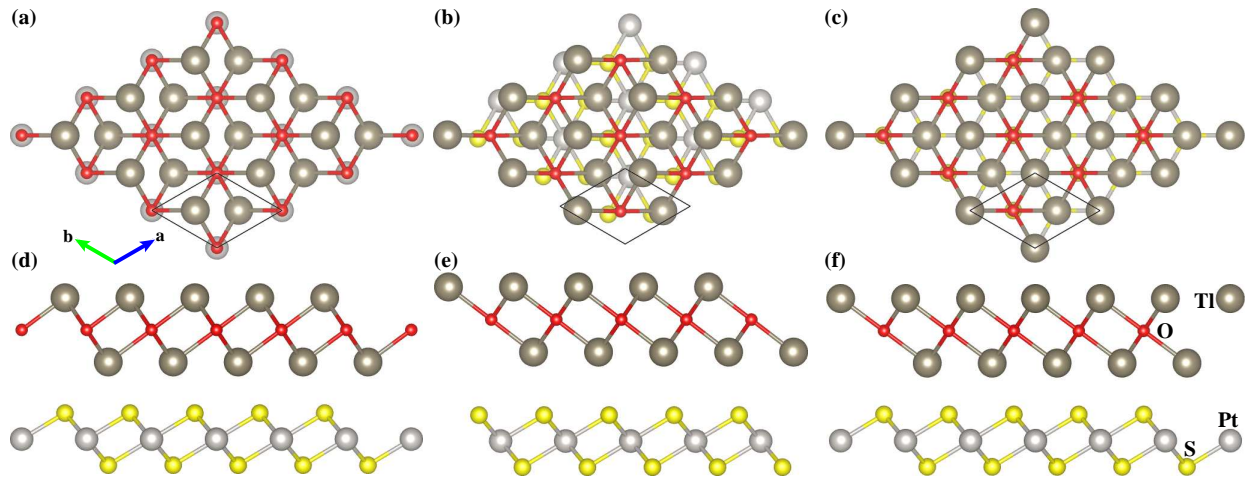


Figure 2: (a-c) Top view of the crystal structure of the  $\text{PtS}_2$  (red),  $\text{Tl}_2\text{O}$  (yellow) and  $\text{Tl}_2\text{O}/\text{PtS}_2$  heterostructure. (d-f) Side view of the crystal structure of the  $\text{PtS}_2$  (red),  $\text{Tl}_2\text{O}$  (yellow) and  $\text{Tl}_2\text{O}/\text{PtS}_2$  heterostructure. The lattice vectors  $a$  and  $b$  are shown in (d).

atoms of  $\text{PtS}_2$  tu

It is pertinent to

to small atomic d

is, for compariso

is used in the res

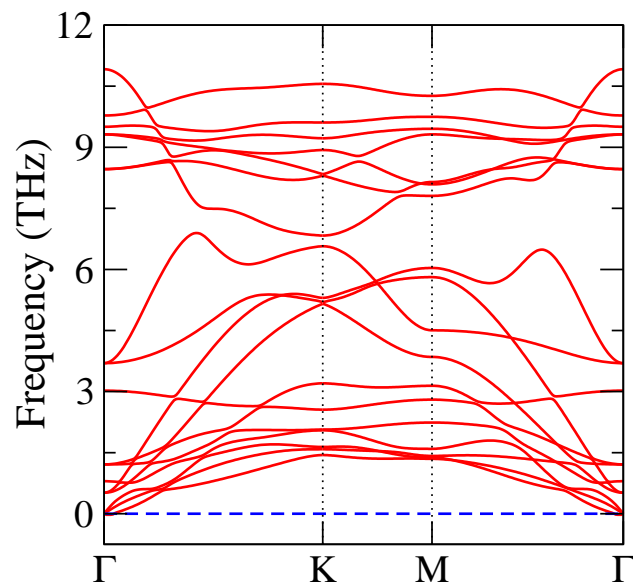


Figure 3: Phonon band structure of the  $\text{Tl}_2\text{O}/\text{PtS}_2$  heterostructure.

We first checked the dynamical stability of the  $\text{Tl}_2\text{O}/\text{PtS}_2$  heterostructure by calculating

the phonon band structure. As displayed in Figure 3, the phonon spectra for the minimum energy configuration does not show any imaginary frequencies, predicting the heterostructure to be stable. Moreover, we find coupling between the acoustic and optical phonons due to the strong interlayer interactions between the constituent systems as discussed below.

To calculate the extent of binding between the constituent systems, we calculate the binding energy (per unit cell as marked in Figure 2) through equation (1),

$$E_b = E(\text{Tl}_2\text{O}/\text{PtS}_2) - E(\text{Tl}_2\text{O}) - E(\text{PtS}_2), \quad (1)$$

where  $E(\text{Tl}_2\text{O}/\text{PtS}_2)$  is the total energy of the heterostructure,  $E(\text{Tl}_2\text{O})$  is the total energy of pristine  $\text{Tl}_2\text{O}$ , and  $E(\text{PtS}_2)$  is the total energy of pristine  $\text{PtS}_2$ . The obtained binding energy of  $-0.38$  eV (per unit cell) shows unusually strong binding between  $\text{Tl}_2\text{O}$  and  $\text{PtS}_2$ , compared to similar vdW heterostructures.<sup>45,46</sup> An interlayer distance of  $2.85 \text{ \AA}$  also supports this observation. As previous studies highlighted the importance of testing different van der Waals density functionals in this realm,<sup>47</sup> we also performed structural relaxation, and subsequently calculated the binding energy for the minimum energy configuration using the optB86b-vdW density functional.<sup>48,49</sup> We obtain similar values using this functional and thus we can confidently categorize strong interlayer interactions in the  $\text{Tl}_2\text{O}/\text{PtS}_2$  heterostructure.

Turning to the electronic and spintronic properties of the  $\text{Tl}_2\text{O}/\text{PtS}_2$  heterostructure, we have calculated the electronic band structure given in Figure 4(a-c). The constituent systems largely preserve their pristine band structures (cf. Figure 1), but we observe a small reduction in the band gap of  $\text{Tl}_2\text{O}$  to a new value of  $0.84$  eV. Significant changes are however observed around the high symmetry gamma point near the Fermi level wherein the energy bands become more parabolic compared to pristine  $\text{Tl}_2\text{O}$  (cf. Figure 4b and Figure 1a). Moreover, we observe an upward shift of the energy bands at the high symmetry gamma point due to the orbital rearrangements caused by the interaction between  $\text{Tl}_2\text{O}$  and  $\text{PtS}_2$ . To investigate this further, we applied a small biaxial tensile strain up to 4% and recalculated the

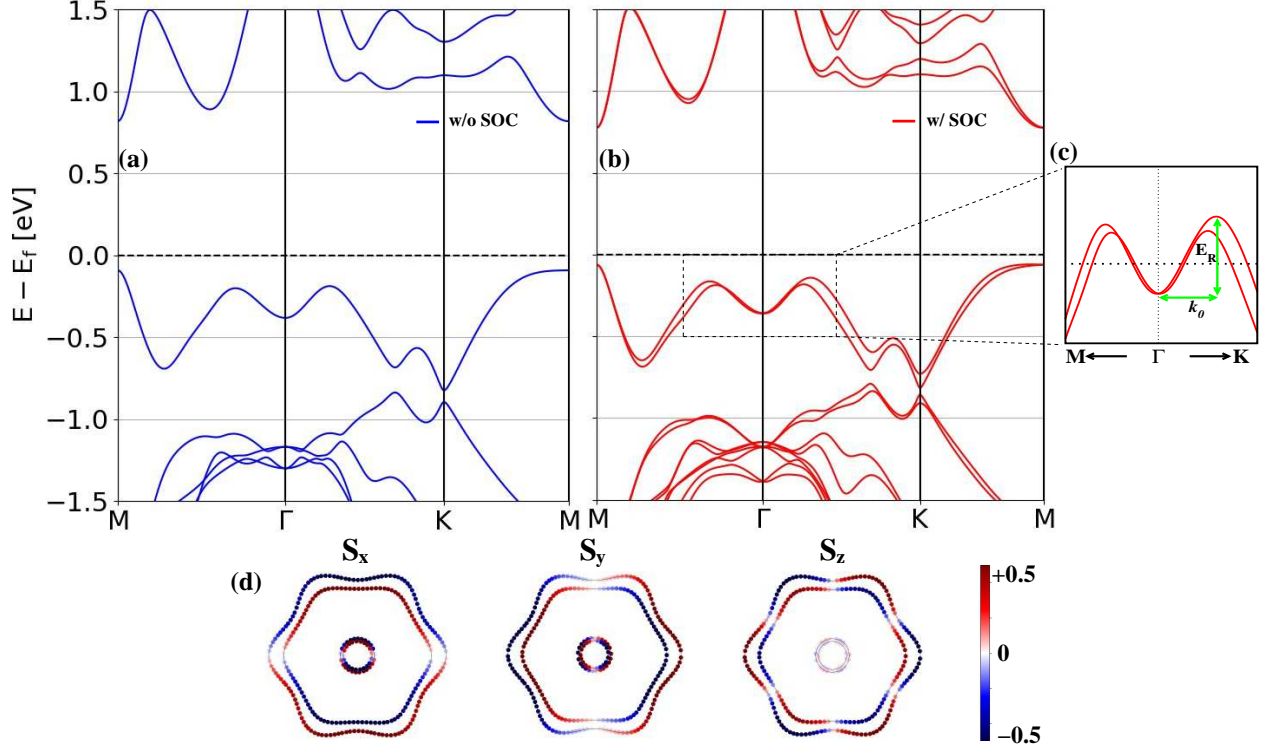


Figure 4: Electronic band structure of  $\text{Tl}_2\text{O}/\text{PtS}_2$  heterostructure (a) without (w/o) SOC and (b) with (w/) SOC, respectively. (c) Zoomed valence band region defining the generalized Rashba-energy  $E_R$  and the momentum-offset  $k_0$ . (d) Fixed-energy spin-contour plots corresponding to dashed black line ( $E = -0.30$  eV) in (c).

electronic band structures (see Supplementary Figure S1). For the increased lattice constant in the strained heterostructure, the interlayer distance between  $\text{Tl}_2\text{O}$  and  $\text{PtS}_2$  was slightly decreased in the structural relaxation (from  $2.85 \text{ \AA}$  to  $2.71 \text{ \AA}$ ). As a result, we observe a minuscule downward shift of the bands at the M-point and an upward shift at the gamma point. Most noticeably, inclusion of spin-orbit coupling show Rashba-type spin-splittings along the momentum-axis (i.e., spin-degenerate band splits into two parabolic bands with opposite polarities) around the high symmetry gamma-point (see Figure 4b and zoomed region in Figure 4c). To confirm this, we plot fixed-energy ( $E = -0.30$  eV) contour plots of the spin-components ( $s_x$ ,  $s_y$  and  $s_z$ ) by setting up a dense 2D k-mesh in the xy-plane (see Figure 4d). The spin textures show clockwise and anticlockwise rotation of electron's spin in traversing from high symmetry  $\text{M} \rightarrow \Gamma \rightarrow \text{K}$  direction in the Brillouin zone validating these observations. We anticipate that the Rashba effect in  $\text{Tl}_2\text{O}/\text{PtS}_2$  heterostructures can be

electrically controlled by applying an external gate voltage. We employ the well-established Rashba Hamiltonian of a 2D-electron gas to describe the electronic dispersion according to equation (2),

$$H_R = \pm \frac{\hbar^2 k_{\parallel}^2}{2m^*} + \alpha_R \vec{\sigma} \cdot (\vec{k}_{\parallel} \times \vec{z}), \quad (2)$$

in which  $k_{\parallel} = (k_x, k_y, 0)$  and  $m^*$  is the in-plane momentum and effective mass of electron, respectively,  $\vec{\sigma}$  is the vector of Pauli matrices and  $\vec{z}$  is the out-of-plane unit vector. The Rashba parameter ( $\alpha_R$ ) for a momentum-split parabolic-dispersion around the high symmetry gamma point, which represents the strength of the spin-orbit coupling, is approximated by  $\alpha_R = 2E_R/k_0$ , whereas  $E_R = \hbar^2 k_0^2/2m^*$  and  $k_0 = m^* \alpha_R/\hbar^2$ . Defining  $E_R$  as the energy difference between the valence band maximum and the band crossing at the  $\Gamma$ -point and  $k_0$  as the momentum offset, as seen in Figure 4c. For the  $\text{Ti}_2\text{O}/\text{PtS}_2$  heterostructure, we obtain large energy difference ( $E_R = 218$  meV) and momentum offset ( $k_0 = 0.057 \text{ \AA}^{-1}$ ) values thus resulting in the Rashba parameter  $\alpha_R = 7.65 \text{ eV \AA}$ . This value is higher than what has been found in the existing literature, which can be seen from our compilation in Table 1. Since the channel material in a typical spin field-effect transistor demands Rashba effect with large  $\alpha_R$  values,  $\text{Ti}_2\text{O}$  in heterostructure with  $\text{PtS}_2$  could be a potential candidate for building spintronics devices.

**Table 1: Rashba spin-splitting parameters of  $\text{Ti}_2\text{O}/\text{PtS}_2$  heterostructure in comparison to previous works.  $E_R$  is energy difference between the valence band maximum and band crossing at the  $\Gamma$ -point,  $k_0$  is the momentum shift and  $\alpha_R$  is the Rashba parameter.**

Case	$E_R(\text{meV})$	$k_0(\text{\AA}^{-1})$	$\alpha_R(\text{eV \AA})$	Reference
$\text{Ti}_2\text{O}/\text{PtS}_2$ Heterostructure	218	0.057	7.65	This work
GaSe/MoSe <sub>2</sub> Heterostructure	31	0.13	0.49	46
PtSe <sub>2</sub> /MoSe <sub>2</sub> Heterostructure	150	0.23	1.30	50
Bi/Ag(111) Surface Alloy	200	0.13	3.05	51
Bulk BiTeI	100	0.052	3.80	15
I-doped PtSe <sub>2</sub>	12.5	0.015	1.70	52
LaOBiS <sub>2</sub>	38	0.025	3.04	53
MoSSe	1.4	0.005	0.53	54

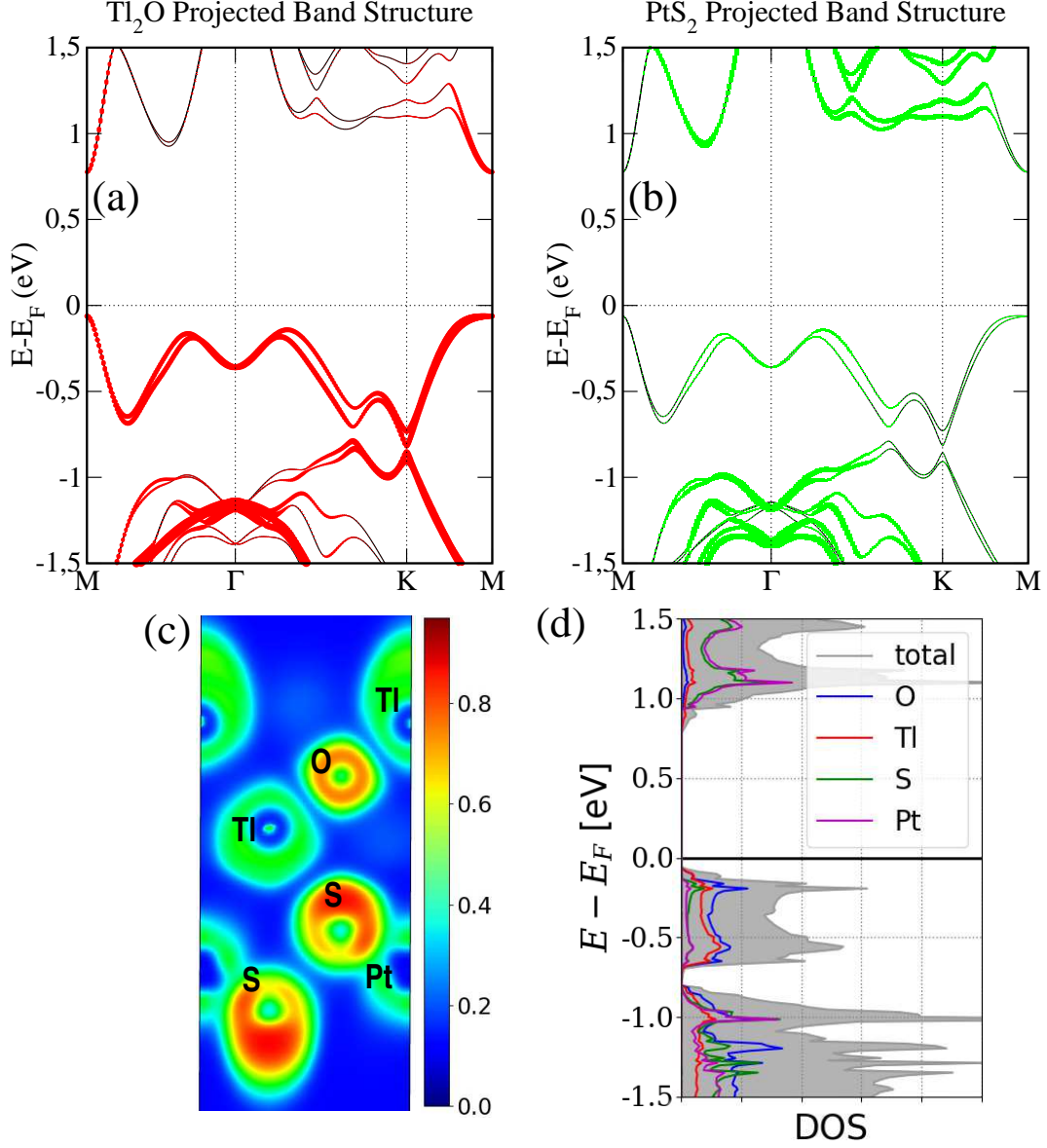


Figure 5: Electronic band structure projected on (a)  $\text{Tl}_2\text{O}$  (b)  $\text{PtS}_2$ . (c) 2D Electron localization function corresponding to the (110)-surface passing through the heterostructure. (d) Total and atom-projected density of states (DOS).

The importance of spin-orbit coupling in engineering the Rashba effect has been highlighted in several studies.<sup>46,50</sup> To gain insights into the underlying mechanism in the  $\text{Tl}_2\text{O}/\text{PtS}_2$  heterostructure responsible for this effect, we scrutinize the layer projected band structures in Figure 5(a-b). Comparing the valence bands of the heterostructure with the individual monolayers in Figure 1, we have found that the top valence band around the gamma point is dominated by  $\text{Tl}_2\text{O}$  but also has contributions from  $\text{PtS}_2$ . Moreover, looking at the atom-

projected DOS given in Figure 5d, despite PtS<sub>2</sub> electronic band dispersion to be present at an energy below  $-0.80$  eV, we observe also small orbital contributions of Pt and S atoms in the energy window of  $-0.25$  eV to  $-0.75$  eV which depicts the same. This means that in the momentum space the two sides of the interface have bands contributing at the same energies around this point. Furthermore, the main contribution to the valence band close to the Fermi level and around the high symmetry gamma point is coming from  $p$ -orbitals, whereas there is mixed  $p$ - and  $d$ -orbital contributions in the conduction band (see Supplementary Figure S2(a-b)). To further examine interlayer interaction, we also analyze the electron localization function (ELF) (see Figure 5c), which shows remarkable contractions of the electron densities for the Tl and S atoms facing the interface (compare to the outer Tl and S atoms in the heterostructure) caused by the induced moments and Pauli repulsion due to the vdW binding. This is much more pronounced than the similar effect discussed for graphene/graphite in Ref.<sup>55</sup> because the vdW interaction between Tl<sub>2</sub>O and PtS<sub>2</sub> in addition to dispersion contains dipole-dipole interactions as becomes evident when comparing the electronegativity for the interfacial atoms (Tl (1.62) and S (2.58)). This large perturbation of the PtS<sub>2</sub> bands around the gamma point gives rise to the interfacial spin-orbit coupling which in turn produces the Rashba effect. However, the ELF clearly shows that there are no bonds formed between Tl<sub>2</sub>O and PtS<sub>2</sub>, therefore we conclude that there is no hybridization between the two materials. Au contraire, our analysis of the physisorption between the materials show that their densities repel each other, which means that these states are separated in real space. Interface states that are separated in real space but locked together in momentum space due to strong physisorption seems to have been found in other 2D heterostructures,<sup>50</sup> but have not been evaluated properly. We suggest that designing strong physisorption in 2D heterostructures could be further explored to realize more and stronger spin physics phenomena.

Finally, to further motivate experimental confirmation of our findings, we have also calculated the Raman spectra of pristine Tl<sub>2</sub>O (in black) and the Tl<sub>2</sub>O/PtS<sub>2</sub> heterostructure

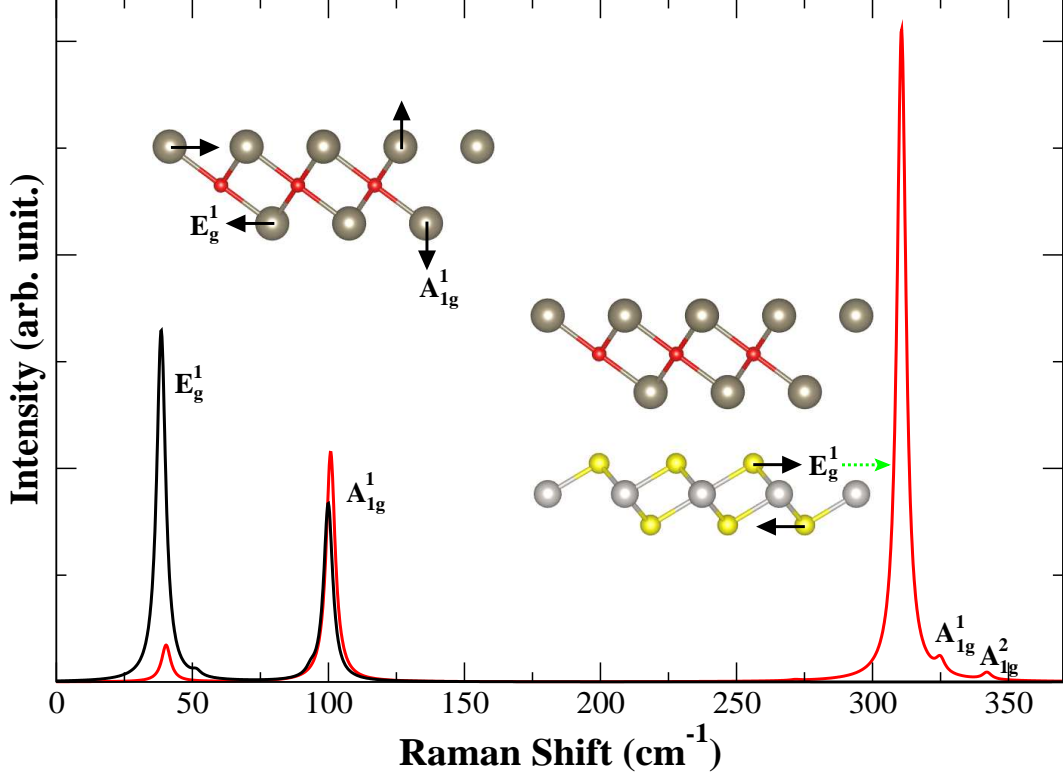


Figure 6: Raman spectra of pristine  $\text{Tl}_2\text{O}$  (black) and  $\text{Tl}_2\text{O}/\text{PtS}_2$  heterostructure (red).

(in red) as shown in Figure 6. For pristine  $\text{Tl}_2\text{O}$ , we observe two characteristic peaks corresponding to the  $E_g^1$  and  $A_{1g}^1$  modes at  $40\text{ cm}^{-1}$  and  $100\text{ cm}^{-1}$ , respectively. The  $E_g^1$  peak of high intensity corresponds to the in-plane vibrational modes of Tl atoms within the 2D sheet, whereas the  $A_{1g}^1$  peaks originate from the out-of-plane Tl atomic vibrations. In the Raman spectra of the  $\text{Tl}_2\text{O}/\text{PtS}_2$  heterostructure, we observe additional peaks corresponding to  $\text{PtS}_2$ , i.e., the  $E_g$  peak at  $310\text{ cm}^{-1}$  and the minuscule  $A_{1g}^1$  and  $A_{1g}^2$  peaks at  $325\text{ cm}^{-1}$  and  $340\text{ cm}^{-1}$ , respectively, belonging to the in-plane and out-of-plane atomic vibration of S atoms which are in complete agreement to the experimental study of Ref.<sup>56</sup> On the other hand, the  $E_g^1$  and  $A_{1g}^1$  peaks belonging to  $\text{Tl}_2\text{O}$  largely preserve their positions albeit with a much smaller intensity of  $E_g^1$  compared to its pristine counterpart. While there can be many factors affecting the Raman spectra (such as structural changes or interlayer spacing), we attribute this change to the strong interlayer interactions between the constituent systems of the heterostructure.

## Conclusion

We performed density functional theory calculations to examine the electronic and spintronic properties of a  $\text{Tl}_2\text{O}/\text{PtS}_2$  heterostructure. Different lateral stackings were carefully tried before arriving at the minimum energy configuration for which the lattice vibrations from the phonon band structure confirm dynamical stability of the heterostructure. We found an unusually high binding energy of -0.38 eV in  $\text{Tl}_2\text{O}/\text{PtS}_2$  heterostructure which shows firm attachment and the presence of strong interlayer interactions between the two materials. While the electronic band structures were essentially preserved in the heterostructure, we discovered Rashba spin-splittings with large energy ( $E_R = 218$  meV) and momentum offset ( $k_0 = 0.057 \text{ \AA}^{-1}$ ) values around the gamma point resulting in the Rashba parameter  $\alpha_R = 7.65 \text{ eV \AA}$ , the highest among similar 2D heterostructures. We discussed the underlying mechanism, i.e., interfacial spin-orbit effects, via the evaluation of the electron localization function, orbital rearrangements and band structure projections and the atom-projected density-of-states calculations. In particular, we shed light on the peculiar feature of band structure alignment in momentum space but separation in real space by analyzing layer-projected band structures. The effect of small biaxial tensile strain was also highlighted in maintaining the characteristic Rashba features of the heterostructure. Finally, to expedite experimental confirmation of our results, we provided the Raman spectra of pristine  $\text{Tl}_2\text{O}$  and  $\text{Tl}_2\text{O}/\text{PtS}_2$  heterostructure with details of different peak positions corresponding to atomic vibrations. Owing to the importance of spin generation, detection, and manipulation in a typical spintronics device, our results provide a promising platform to harness spin degree of freedom in 2D heterostructures by employing interfacial spin-orbit effects.

## Acknowledgement

We thank Knut och Alice Wallenberg foundation, Kempestiftelserna and Interreg Nord for financial support. The computations were enabled by resources provided by the Swedish

National Infrastructure for Computing (SNIC) at HPC2N and NSC partially funded by the Swedish Research Council through grant agreement no. 2018-05973.

## Competing Interests

The Authors declare no competing financial or non-financial interests.

## Data Availability

The data that support the findings of this study are available from the corresponding author upon reasonable request.

## Author Contribution

S. Sattar performed the calculations, S. Sattar and J. A. Larsson analysed the results. All authors reviewed the manuscript.

## References

- (1) Yan, W.; Txoperena, O.; Llopis, R.; Dery, H.; Hueso, L. E.; Casanova, F. A Two-Dimensional Spin Field-Effect Switch. *Nature Communications* **2016**, *7*, 1–6.
- (2) Radisavljevic, B.; Radenovic, A.; Brivio, J.; Giacometti, V.; Kis, A. Single-Layer MoS<sub>2</sub> Transistors. *Nature Nanotechnology* **2011**, *6*, 147–150.
- (3) Zeng, H.; Dai, J.; Yao, W.; Xiao, D.; Cui, X. Valley Polarization in MoS<sub>2</sub> Monolayers by Optical Pumping. *Nature Nanotechnology* **2012**, *7*, 490–493.
- (4) Ghiasi, T. S.; Ingla-Aynés, J.; Kaverzin, A. A.; van Wees, B. J. Large Proximity-Induced Spin Lifetime Anisotropy in Transition-Metal Dichalcogenide/Graphene Heterostructures. *Nano Letters* **2017**, *17*, 7528–7532.

- (5) Bychkov, Y. A.; Rashba, É. Properties of a 2D Electron Gas with Lifted Spectral Degeneracy. *JETPL* **1984**, *39*, 78.
- (6) Manchon, A.; Koo, H. C.; Nitta, J.; Frolov, S.; Duine, R. New perspectives for Rashba spin-orbit coupling. *Nature Materials* **2015**, *14*, 871–882.
- (7) LaShell, S.; McDougall, B.; Jensen, E. Spin Splitting of an Au (111) Surface State Band Observed with Angle Resolved Photoelectron Spectroscopy. *Physical Review Letters* **1996**, *77*, 3419.
- (8) Koroteev, Y. M.; Bihlmayer, G.; Gayone, J.; Chulkov, E.; Blügel, S.; Echenique, P. M.; Hofmann, P. Strong Spin-Orbit Splitting on Bi Surfaces. *Physical Review Letters* **2004**, *93*, 046403.
- (9) Kimura, A.; Krasovskii, E.; Nishimura, R.; Miyamoto, K.; Kadono, T.; Kanomaru, K.; Chulkov, E.; Bihlmayer, G.; Shimada, K.; Namatame, H., et al. Strong Rashba-Type Spin Polarization of the Photocurrent From Bulk Continuum States: Experiment and Theory for Bi(111). *Physical Review Letters* **2010**, *105*, 076804.
- (10) Su, S. H.; Chuang, P. Y.; Chen, S. W.; Chen, H. Y.; Tung, Y.; Chen, W.-C.; Wang, C.-H.; Yang, Y.-W.; Huang, J. C. A.; Chang, T.-R., et al. Selective Hydrogen Etching Leads to 2D Bi(111) Bilayers on Bi<sub>2</sub>Se<sub>3</sub>: Large Rashba Splitting in Topological Insulator Heterostructure. *Chemistry of Materials* **2017**, *29*, 8992–9000.
- (11) Hirahara, T.; Nagao, T.; Matsuda, I.; Bihlmayer, G.; Chulkov, E.; Koroteev, Y. M.; Echenique, P.; Saito, M.; Hasegawa, S. Role of Spin-Orbit Coupling and Hybridization Effects in the Electronic Structure of Ultrathin Bi Films. *Physical Review Letters* **2006**, *97*, 146803.
- (12) Hochstrasser, M.; Tobin, J.; Rotenberg, E.; Kevan, S. Spin-Resolved Photoemission of Surface States of W(110)-(1×1) h. *Physical Review Letters* **2002**, *89*, 216802.

- (13) Dil, J. H.; Meier, F.; Lobo-Checa, J.; Patthey, L.; Bihlmayer, G.; Osterwalder, J. Rashba-Type Spin-Orbit Splitting of Quantum Well States in Ultrathin Pb Films. *Physical Review Letters* **2008**, *101*, 266802.
- (14) Varykhalov, A.; Marchenko, D.; Scholz, M.; Rienks, E.; Kim, T.; Bihlmayer, G.; Sánchez-Barriga, J.; Rader, O. Ir(111) Surface State with Giant Rashba Splitting Persists Under Graphene in Air. *Physical Review Letters* **2012**, *108*, 066804.
- (15) Ishizaka, K.; Bahramy, M.; Murakawa, H.; Sakano, M.; Shimojima, T.; Sonobe, T.; Koizumi, K.; Shin, S.; Miyahara, H.; Kimura, A.; Miyamoto, K.; Okuda, T.; Namatame, H.; Taniguchi, M.; Arita, R.; Nagaosa, N.; Kobayashi, K.; Murakami, Y.; Kumai, R.; Kaneko, Y.; Onose, Y.; Tokura, Y. Giant Rashba-Type Spin Splitting in Bulk BiTeI. *Nature Materials* **2011**, *10*, 521–526.
- (16) Di Sante, D.; Barone, P.; Bertacco, R.; Picozzi, S. Electric Control of the Giant Rashba Effect in Bulk GeTe. *Advanced Materials* **2013**, *25*, 509–513.
- (17) Sakano, M.; Bahramy, M.; Katayama, A.; Shimojima, T.; Murakawa, H.; Kaneko, Y.; Malaeb, W.; Shin, S.; Ono, K.; Kumigashira, H., et al. Strongly Spin-Orbit Coupled Two-Dimensional Electron Gas Emerging Near the Surface of Polar Semiconductors. *Physical Review Letters* **2013**, *110*, 107204.
- (18) Feng, Y.; Jiang, Q.; Feng, B.; Yang, M.; Xu, T.; Liu, W.; Yang, X.; Arita, M.; Schiwer, E. F.; Shimada, K., et al. Rashba-Like Spin Splitting Along Three Momentum Directions in Trigonal Layered PtBi<sub>2</sub>. *Nature Communications* **2019**, *10*, 1–8.
- (19) Niesner, D.; Wilhelm, M.; Levchuk, I.; Osvet, A.; Shrestha, S.; Batentschuk, M.; Brabec, C.; Fauster, T. Giant Rashba Splitting in CH<sub>3</sub>NH<sub>3</sub>PbBr<sub>3</sub> Organic-Inorganic Perovskite. *Physical Review Letters* **2016**, *117*, 126401.
- (20) Niesner, D.; Hauck, M.; Shrestha, S.; Levchuk, I.; Matt, G. J.; Osvet, A.; Batentschuk, M.; Brabec, C.; Weber, H. B.; Fauster, T. Structural Fluctuations Cause

- Spin-Split States in Tetragonal  $(\text{CH}_3\text{NH}_3)\text{PbI}_3$  as Evidenced by the Circular Photogalvanic Effect. *Proceedings of the National Academy of Sciences* **2018**, *115*, 9509–9514.
- (21) Zhai, Y.; Baniya, S.; Zhang, C.; Li, J.; Haney, P.; Sheng, C.-X.; Ehrenfreund, E.; Vardeny, Z. V. Giant Rashba Splitting in 2D Organic-Inorganic Halide Perovskites Measured by Transient Spectroscopies. *Science Advances* **2017**, *3*, e1700704.
- (22) Zhu, Z.-H.; Levy, G.; Ludbrook, B.; Veenstra, C.; Rosen, J.; Comin, R.; Wong, D.; Dosanjh, P.; Ubaldini, A.; Syers, P., et al. Rashba Spin-Splitting Control at the Surface of the Topological Insulator  $\text{Bi}_2\text{Se}_3$ . *Physical Review Letters* **2011**, *107*, 186405.
- (23) King, P.; Hatch, R. C.; Bianchi, M.; Ovsyannikov, R.; Lupulescu, C.; Landolt, G.; Slomski, B.; Dil, J.; Guan, D.; Mi, J., et al. Large Tunable Rashba Spin Splitting of a Two-Dimensional Electron Gas in  $\text{Bi}_2\text{Se}_3$ . *Physical Review Letters* **2011**, *107*, 096802.
- (24) Zhou, J.-J.; Feng, W.; Zhang, Y.; Yang, S. A.; Yao, Y. Engineering Topological Surface States and Giant Rashba Spin Splitting in  $\text{BiTeI}/\text{Bi}_2\text{Te}_3$  Heterostructures. *Scientific Reports* **2014**, *4*, 3841.
- (25) Lin, W.; Li, L.; Doğan, F.; Li, C.; Rotella, H.; Yu, X.; Zhang, B.; Li, Y.; Lew, W. S.; Wang, S., et al. Interface-Based Tuning of Rashba Spin-Orbit Interaction in Asymmetric Oxide Heterostructures with 3d Electrons. *Nature Communications* **2019**, *10*, 1–7.
- (26) Yao, W.; Wang, E.; Huang, H.; Deng, K.; Yan, M.; Zhang, K.; Miyamoto, K.; Okuda, T.; Li, L.; Wang, Y., et al. Direct Observation of Spin-Layer Locking by Local Rashba Effect in Monolayer Semiconducting  $\text{PtSe}_2$  Film. *Nature Communications* **2017**, *8*, 1–6.
- (27) Khokhriakov, D.; Hoque, A. M.; Karpiak, B.; Dash, S. P. Gate-Tunable Spin-Galvanic Effect in Graphene-Topological Insulator Van der Waals Heterostructures at Room Temperature. *Nature Communications* **2020**, *11*, 1–7.

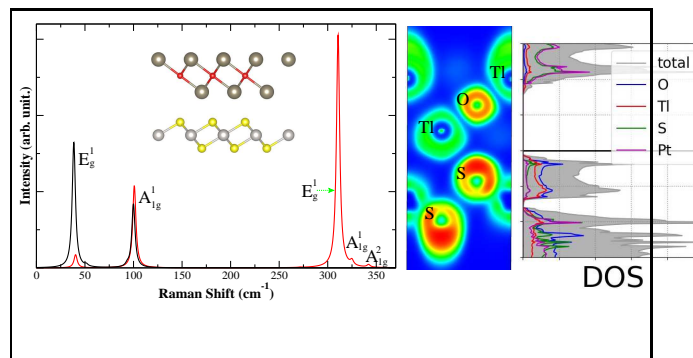
- (28) Ma, Y.; Kuc, A.; Heine, T. Single-layer  $\text{Tl}_2\text{O}$ : A Metal-Shrouded 2D Semiconductor With High Electronic Mobility. *Journal of the American Chemical Society* **2017**, *139*, 11694–11697.
- (29) Li, J.-H.; Wu, J.; Yu, Y.-X. Theoretical Exploration of Single-Layer  $\text{Tl}_2\text{O}$  as a Catalyst in Lithium–Oxygen Battery Cathodes. *The Journal of Physical Chemistry C* **2020**, *124*, 9089–9098.
- (30) Xu, X.; Ma, Y.; Zhang, T.; Lei, C.; Huang, B.; Dai, Y. Nonmetal-Atom-Doping-Induced Valley Polarization in Single-Layer  $\text{Tl}_2\text{O}$ . *The Journal of Physical Chemistry Letters* **2019**, *10*, 4535–4541.
- (31) Wang, C.; Wei, S.; Gao, G. Theoretical Investigation of Metal-Shrouded  $\text{Tl}_2\text{O}$  Monolayers: Pudding-Mold-Type Band Structure and Thermoelectric Performance. *ACS Applied Nano Materials* **2019**, *2*, 4061–4066.
- (32) Huang, H.; Xing, G.; Fan, X.; Singh, D. J.; Zheng, W. Layered  $\text{Tl}_2\text{O}$ : A Model Thermoelectric Material. *Journal of Materials Chemistry C* **2019**, *7*, 5094–5103.
- (33) Sajjad, M.; Singh, N.; Sattar, S.; De Wolf, S.; Schwingenschlögl, U. Ultralow Lattice Thermal Conductivity and Thermoelectric Properties of Monolayer  $\text{Tl}_2\text{O}$ . *ACS Applied Energy Materials* **2019**, *2*, 3004–3008.
- (34) Ma, Y.; Kou, L.; Du, A.; Huang, B.; Dai, Y.; Heine, T. Conduction-Band Valley Spin Splitting in Single-Layer  $\text{H-Tl}_2\text{O}$ . *Physical Review B* **2018**, *97*, 035444.
- (35) Gruznev, D.; Bondarenko, L.; Tupchaya, A.; Mihalyuk, A.; Ereemeev, S.; Zotov, A.; Saranin, A. Thallene: Graphene-Like Honeycomb Lattice of Tl Atoms Frozen on Single-Layer  $\text{NiSi}_2$ . *2D Materials* **2020**, *7*, 045026.
- (36) Blöchl, P. E. Projector Augmented-Wave Method. *Phys. Rev. B* **1994**, *50*, 17953–17979.

- (37) Kresse, G.; Furthmüller, J. Efficient Iterative Schemes for Ab Initio Total-Energy Calculations Using a Plane-Wave Basis Set. *Phys. Rev. B* **1996**, *54*, 11169–11186.
- (38) Kresse, G.; Joubert, D. From Ultrasoft Pseudopotentials to the Projector Augmented-Wave Method. *Phys. Rev. B* **1999**, *59*, 1758–1775.
- (39) Grimme, S.; Antony, J.; Ehrlich, S.; Krieg, H. A Consistent and Accurate Ab Initio Parametrization of Density Functional Dispersion Correction (DFT-D) For the 94 Elements H-Pu. *The Journal of Chemical Physics* **2010**, *132*, 154104.
- (40) Togo, A.; Tanaka, I. First Principles Phonon Calculations in Materials Science. *Scripta Materialia* **2015**, *108*, 1–5.
- (41) Fonari, A.; Stauffer, S. vasp\_raman.py. **2013**, <https://github.com/raman-sc/VASP/>.
- (42) Herath, U.; Tavadze, P.; He, X.; Bousquet, E.; Singh, S.; Muñoz, F.; Romero, A. H. PyProcar: A Python Library for Electronic Structure Pre/Post-Processing. *Computer Physics Communications* **2020**, *251*, 107080.
- (43) Hunter, J. D. Matplotlib: A 2D Graphics Environment. *Computing in Science Engineering* **2007**, *9*, 90–95.
- (44) Zhao, Y.; Qiao, J.; Yu, P.; Hu, Z.; Lin, Z.; Lau, S. P.; Liu, Z.; Ji, W.; Chai, Y. Extraordinarily strong interlayer interaction in 2D layered PtS<sub>2</sub>. *Advanced materials* **2016**, *28*, 2399–2407.
- (45) Nguyen, C. V.; Bui, H.; Nguyen, T. D.; Pham, K. D. Controlling Electronic Properties of PtS<sub>2</sub>/InSe van der Waals Heterostructure via External Electric Field and Vertical strain. *Chemical Physics Letters* **2019**, *724*, 1–7.
- (46) Zhang, Q.; Schwingenschlögl, U. Rashba Effect and Enriched Spin-Valley Coupling in GaX/MX<sub>2</sub> ( $M = \text{Mo, W}$ ;  $X = \text{S, Se, Te}$ ) Heterostructures. *Phys. Rev. B* **2018**, *97*, 155415.

- (47) Zhu, J.; Schwingenschloegl, U. Silicene on MoS<sub>2</sub>: Role of the Van der Waals Interaction. *2D Materials* **2015**, *2*, 045004.
- (48) Klimeš, J.; Bowler, D. R.; Michaelides, A. Chemical Accuracy For the Van der Waals Density Functional. *Journal of Physics: Condensed Matter* **2009**, *22*, 022201.
- (49) Klimeš, J.; Bowler, D. R.; Michaelides, A. Van der Waals Density Functionals Applied to Solids. *Phys. Rev. B* **2011**, *83*, 195131.
- (50) Xiang, L.; Ke, Y.; Zhang, Q. Tunable Giant Rashba-Type Spin Splitting in PtSe<sub>2</sub>/MoSe<sub>2</sub> Heterostructure. *Applied Physics Letters* **2019**, *115*, 203501.
- (51) Ast, C. R.; Henk, J.; Ernst, A.; Moreschini, L.; Falub, M. C.; Pacilé, D.; Bruno, P.; Kern, K.; Grioni, M. Giant Spin Splitting Through Surface Alloying. *Physical Review Letters* **2007**, *98*, 186807.
- (52) Absor, M. A. U.; Santoso, I.; Harsojo; Abraha, K.; Kotaka, H.; Ishii, F.; Saito, M. Strong Rashba Effect in the Localized Impurity States of Halogen-Doped Monolayer PtSe<sub>2</sub>. *Physical Review B* **2018**, *97*, 205138.
- (53) Liu, Q.; Guo, Y.; Freeman, A. J. Tunable Rashba Effect in Two-Dimensional LaOBiS<sub>2</sub> Films: Ultrathin Candidates For Spin Field Effect Transistors. *Nano Letters* **2013**, *13*, 5264–5270.
- (54) Li, F.; Wei, W.; Zhao, P.; Huang, B.; Dai, Y. Electronic and Optical Properties of Pristine and Vertical and Lateral Heterostructures of Janus MoSSe and WSSe. *Journal of Physical Chemistry Letters* **2017**, *8*, 5959–5965.
- (55) Koumpouras, K.; Larsson, J. A. Distinguishing Between Chemical Bonding and Physical Binding Using Electron Localization Function (ELF). *Journal of Physics: Condensed Matter* **2020**, *32*, 315502.

- (56) Pi, L.; Li, L.; Hu, X.; Zhou, S.; Li, H.; Zhai, T. Temperature Dependence of Raman Responses of Few-Layer PtS<sub>2</sub>. *Nanotechnology* **2018**, *29*, 505709.

# Graphical TOC Entry



# Supporting Information

## Rashba Effect and Raman Spectra of Monolayer $\text{Ti}_2\text{O}/\text{PtS}_2$ Heterostructure

Shahid Sattar\* and J. Andreas Larsson\*

*Applied Physics, Division of Materials Science, Department of Engineering Sciences and  
Mathematics, Luleå University of Technology, Luleå SE-97187, Sweden*

E-mail: shahid.sattar@ltu.se; andreas.1.larsson@ltu.se

Phone: +46 (0)920 491930

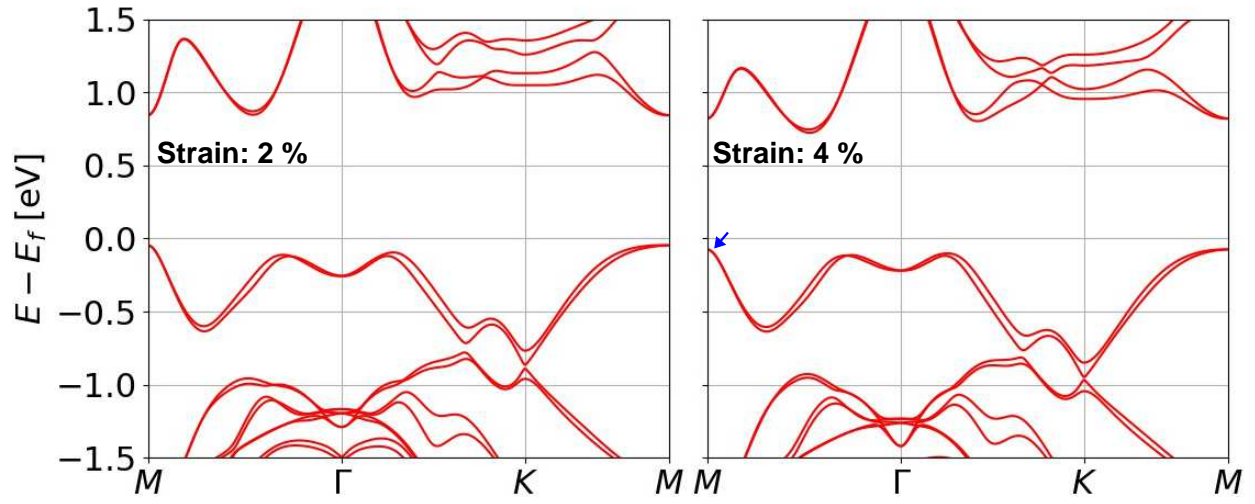


Figure S1: Effect of strain on the electronic band structure of monolayer  $\text{Tl}_2\text{O}/\text{PtS}_2$  heterostructure.

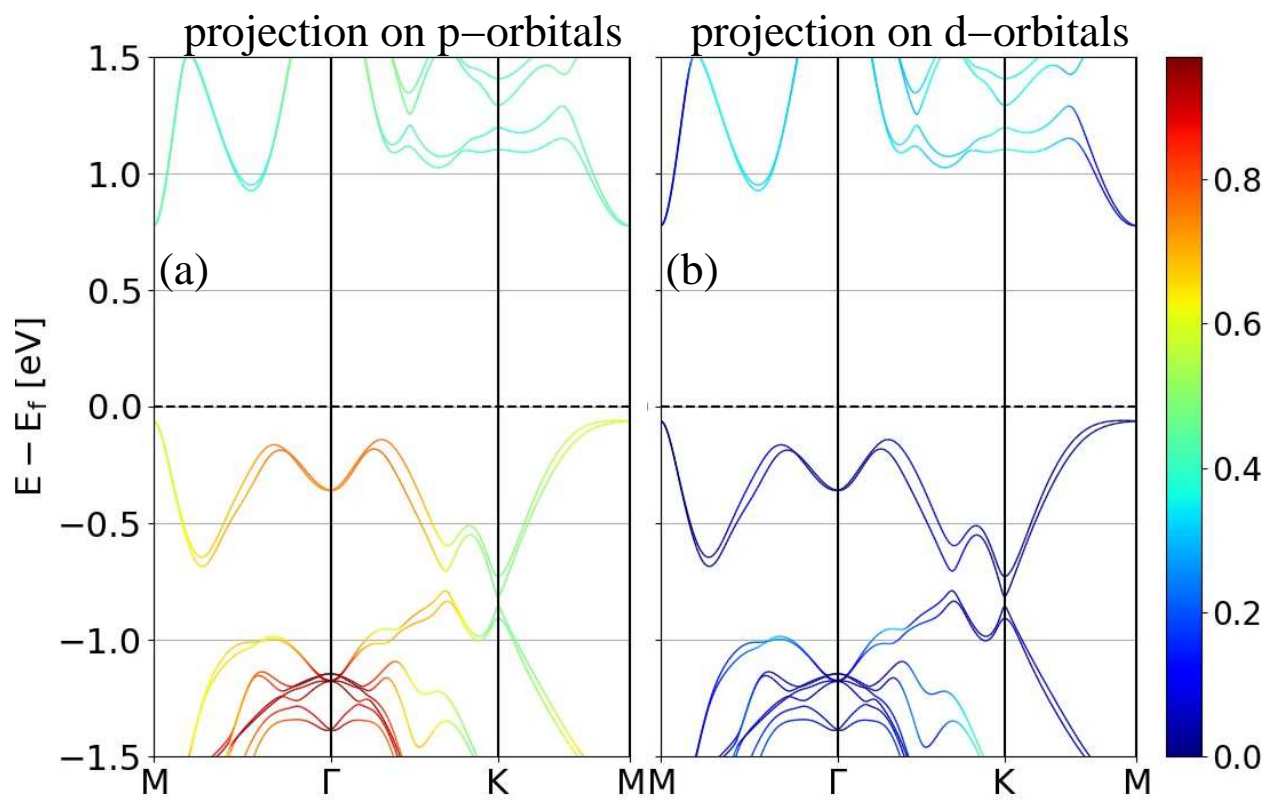


Figure S2: Atomic orbital projected band structures of the  $\text{Tl}_2\text{O}/\text{PtS}_2$  heterostructure.